

Article

# Data-Driven Control Techniques for Renewable Energy Conversion Systems: Wind Turbine and Hydroelectric Plants

Silvio Simani\*, Stefano Alvisi and Mauro Venturini

Dipartimento di Ingegneria, Università degli Studi di Ferrara. Via Saragat 1E, Ferrara (FE) 44122, Italy.  
{silvio.simani,stefano.alvisi,mauro.venturini}@unife.it

\* Corresponding author. Correspondence: silvio.simani@unife.it; Tel.: +39-0532-97-4844

**Abstract:** The interest on the use of renewable energy resources is increasing, especially towards wind and hydro powers, which should be efficiently converted into electric energy via suitable technology tools. To this aim, data-driven control techniques represent viable strategies that can be employed for this purpose, due to the features of these nonlinear dynamic processes working over a wide range of operating conditions, driven by stochastic inputs, excitations and disturbances. Some of the considered methods, such as fuzzy and adaptive self-tuning controllers, were already verified on wind turbine systems, and similar advantages may thus derive from their appropriate implementation and application to hydroelectric plants. These issues represent the key features of the work, which provides some guidelines on the design and the application of these control strategies to these energy conversion systems. The working conditions of these systems will be also taken into account in order to highlight the reliability and robustness characteristics of the developed control strategies, especially interesting for remote and relatively inaccessible location of many installations.

**Keywords:** Wind turbine system; hydroelectric plant simulator; model-based control; data-driven approach; self-tuning control; robustness and reliability

## 1. Introduction

The trend to reduce the use of fossil fuels, motivated by the need to meet greenhouse gas emission limits, has driven much interest on renewable energy resources, in order also to cover global energy requirements. Wind turbine systems, which now represent a mature technology, have had much more development with respect to other energy conversion systems, *e.g.* for biomass, solar, and hydropower [1]. In particular, hydroelectric plants present interesting energy conversion potentials, with commonalities and contrast with respect to wind turbine installations [2–4].

One common aspect regarding the design of the renewable energy conversion system concerns the conversion efficiency. However, as wind and hydraulic resources are free, the key point is represented by the minimisation of the cost per kWh, also considering the lifetime of the deployments. Moreover, by taking into account that the cost of control system technology (*i.e.* sensors, actuators, computer, software) is relatively lower than the one of the renewable energy converter, the control system should aim at increasing the energy conversion capacity of the given plant [5].

The paper focuses on the development and the comparison of control techniques applied to a wind turbine system and a hydroelectric plant, by using a wind turbine benchmark and a hydroelectric simulator, respectively. The former process was proposed for the purpose of an international competition started in 2009 [6], whilst the latter system was developed by the same authors but with different purpose [7]. In fact, these simulators represent high-fidelity representations of realistic processes, developed for the validation and the verification of advanced control techniques. More general investigations of these plants and their components are addressed in [8] and [9], respectively, even if their structures were analysed for different purpose and applications.

37 With reference to wind turbine systems, can implement their regulation via 'passive' control  
38 methods, such as the plants with fixed-pitch, and stall control machines. These systems may not use  
39 any pitch control mechanism or rely on simple rotational speed control [6]. On the other hand, wind  
40 turbine rotors exploiting adjustable pitch systems are often exploited to overcome the limitations  
41 due to the simple blade stall, and to improve the converted power [10]. Large wind turbines can  
42 implement another control technique modifying the yaw angle, which is used to orient the rotor  
43 towards the wind direction [10].

44 On the other hand, regarding hydroelectric plants, it is worth noting that a limited number of  
45 works have addressed the application of advanced control techniques [11]. In fact, a high-fidelity  
46 mathematical description of these processes can be difficult to be achieved in practice. Some  
47 contributions took into account the elastic water effects, even if the nonlinear dynamics are linearised  
48 around an operating condition. Moreover, other papers proposed different mathematical models  
49 together with the strategies exploited to control these systems [12]. In the same way, linear and  
50 nonlinear dynamic processes with different regulation strategies are also proposed [13]. In particular,  
51 a fuzzy controller that needs for the proper design of the membership functions was proposed in [14].  
52 On the other hand, the paper [12] developed an advanced controller combining four control schemes  
53 that rely on adaptive, fuzzy and neural network regulators.

54 Finally, regarding joint wind-hydro deployments, some more recent works analysed the  
55 problem of frequency control of isolated systems [15,16], which is not addressed in this paper.

56 After these consideration, the main contribution of the paper aims at providing some guidelines  
57 on the design and the application of data-driven and self-tuning control strategies to two energy  
58 conversion systems. Some of these techniques were already verified on wind turbine systems, and  
59 important advantages may thus derive from the appropriate implementation of the same control  
60 methods for hydroelectric plants. In fact, it seems that investigations related with both wind and  
61 hydraulic energies present a reduced number of common aspects, thus leading to little exchange  
62 and share of possible common points. This consideration is particularly valid with reference to  
63 the more established wind area when compared to hydroelectric systems. Moreover, it analyses  
64 the application of the different control solutions to these energy conversion systems. In particular,  
65 the work introduces some kind of common rules for tuning the different controllers, for both wind  
66 turbine and hydroelectric plants. Therefore, the paper shows that the parameters of these controllers  
67 are obtained by exploiting the same tuning strategies. This represents the feature of this study. The  
68 common parts and the working conditions of these energy conversion systems will be also taken into  
69 account in order to highlight the reliability and robustness characteristics of the developed control  
70 strategies.

71 Finally, the paper has the following structure. Section 2 summarises the simulation models used  
72 for describing the accurate behaviour of the dynamic processes. In particular, similar functional  
73 parts that characterise the processes under investigation will be highlighted, as they lead to similar  
74 design rules, illustrated in Section 3. To this aim, Section 3 summarises the design of the proposed  
75 control techniques, taking into account the available tools. In Section 4, these control strategies  
76 are implemented and compared, with respect to the achievable reliability and robustness features.  
77 Section 5 ends the paper summarising the main achievements of the paper, and drawing some  
78 concluding remarks.

## 79 2. Simulator Models and Reference Governors

80 This section recalls the basic structure and the common points of the simulators used for  
81 describing the wind turbine and the hydroelectric processes considered in this paper.

82 This work considers a horizontal-axis wind turbine device, as nowadays it represents the most  
83 common type of installation for large-scale deployments. Moreover, this three-bladed wind turbine  
84 follows the principle that the wind power activates its blades, thus producing the rotation of the low  
85 speed rotor shaft. This rotational speed required by the electric generator is increased via a gear-box

86 with a drive–train. More details on this simulator are available in [6]. The schematic diagram of  
 87 this benchmark that helps to recall its main variables and function blocks developed in the Simulink  
 88 environment is depicted in Fig. 1, thus showing also its working principles.

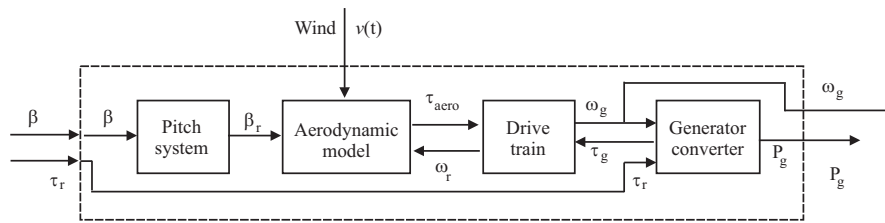


**Figure 1.** Block diagram of the wind turbine simulator.

89 The wind turbine simulator has 2 controlled outputs, *i.e.* the generator rotational speed  $\omega_g(t)$   
 90 and its generated power  $P_g(t)$ . The wind turbine model is controlled by means of two actuated  
 91 inputs, *i.e.* the generator torque  $\tau_g(t)$  and the blade pitch angle  $\beta(t)$ . The latter signal controls the  
 92 blade actuators, which are implemented by a hydraulic circuit [6].

Several other measurements are acquired from the wind turbine benchmark: the signal  $\omega_r(t)$  represents the rotor speed and  $\tau_r(t)$  is the reference torque. Moreover, aerodynamic torque signal  $\tau_{aero}(t)$  is computed from the wind speed  $v(t)$ , which is usually available with limited accuracy. On the other hand, the aerodynamic torque  $\tau_{aero}(t)$  depends on the power coefficient  $C_p$ , as shown by Eq. (1):

$$\tau_{aero}(t) = \frac{\rho A C_p(\beta(t), \lambda(t)) v^3(t)}{2 \omega_r(t)} \quad (1)$$

93  $\rho$  being air density,  $A$  the area swept by the turbine blades during their rotation, whilst  $\lambda(t)$  is the  
 94 tip–speed ratio of the blade. The nonlinear relations of Eq. (1) is represented in Figure 2, which is  
 95 depicted for different values of  $\lambda(t)$ ,  $v(t)$  and  $\beta(t)$ .

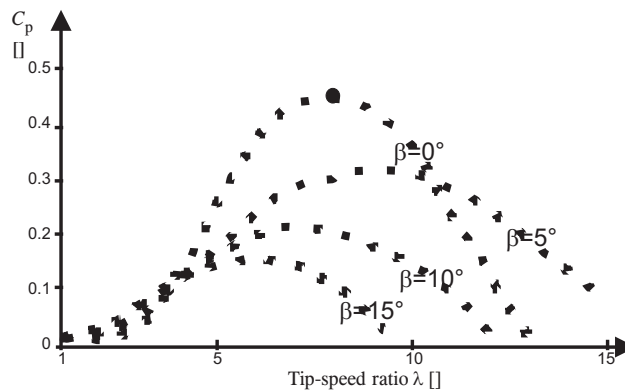


**Figure 2.** Example of the power coefficient function.

96 It is worth noting the mathematical relation of Eq. (1) representing the driving force of the  
 97 wind turbine process, whose formulation will be similar for the hydroelectric plant, as shown in  
 98 the following.

The overall continuous–time representation of the wind turbine benchmark can be represented via Eq. (2):

$$\begin{cases} \dot{x}(t) = f_c(x(t), u(t)) \\ y(t) = x(t) \end{cases} \quad (2)$$

99 with  $u(t) = [\tau_r(t) \beta(t)]^T$  and  $y(t) = [\omega_g(t) P_g(t)]^T$ .  $f_c(\cdot)$  is described by means of a continuous-time  
 100 nonlinear function that will be exploited for representing the complete dynamic behaviour of the  
 101 controlled process. Moreover, since this paper will analyse several data-driven control approaches,  
 102 this system will be used to acquire  $N$  sampled data sequences  $u(k)$  and  $y(k)$ , with  $k = 1, 2, \dots, N$   
 103 from a realistic wind turbine plant [6].

104 Finally, the wind turbine simulator includes a control system that maintains the generator speed  
 105  $\omega_g(t)$  at its nominal value  $\omega_{nom} = 1551,76rpm$ , and the generated power  $P_g(t)$  near to the rated power  
 106  $P_r = 4.8MW$ . This is achieved by properly changing both  $\beta$  and  $\tau_g$ , depending on the operating  
 107 conditions, which move the wind turbine system to the partial load to the full load working regions  
 108 (operating regions 2 and 3, respectively) [6].

109 On the other hand, the hydroelectric plant considered in this work consists of a high water head  
 110 and a long penstock, which includes also upstream and downstream surge tanks, with a Francis  
 111 hydraulic turbine [17], as recalled in Fig. 3. The hydroelectric simulator consists of a reservoir with  
 112 water level  $H_R$ , an upstream water tunnel with cross-section area  $A_1$  and length  $L_1$ , an upstream surge  
 113 tank with cross-section area  $A_2$  and water level  $H_2$  of appropriate dimensions. A downstream surge  
 114 tank with cross-section area  $A_4$  and water level  $H_4$  follows, ending with a downstream tail water  
 115 tunnel of cross-section area  $A_5$  and length  $L_5$ . Moreover, between the Francis hydraulic turbine and  
 116 the two surge tanks, there is a penstock with cross-section area  $A_3$  and length  $L_3$ . Finally, Fig. 3  
 117 highlights a tail water lake with level  $H_T$ . The levels  $H_R$  and  $H_T$  of the reservoir and the lake water,  
 118 respectively, are assumed to be constants.

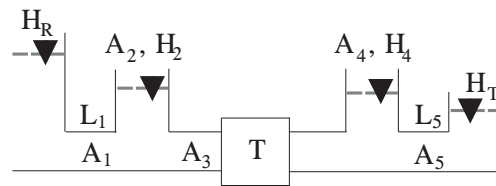


Figure 3. Overall scheme of the hydroelectric process.

119 The mathematical description of the pure hydraulic system, which does not include the Francis  
 120 hydraulic turbine, can be found in [18,19]. This model was modified by the authors in order to  
 121 consider the the Francis turbine [7].

In the following, the complete model of the hydroelectric system is recalled, in terms of the  
 variable  $h$ , which represents the water pressure relative deviation, whilst  $q$  is the flow rate relative  
 deviation. More details can be found in [7]. Therefore, the overall model of the hydroelectric  
 simulator is described by the relations of Eq. (3), which express the non-dimensional variables with  
 respect to their relative deviations:

$$\begin{cases} \frac{Q}{Q_r} = 1 + q_t \\ \frac{H}{H_r} = 1 + h_t \\ \frac{n}{n_r} = 1 + x \\ G = 1 + y \end{cases} \quad (3)$$

122 with  $q_t$  is the turbine flow rate relative deviation,  $h_t$  the turbine water pressure relative deviation,  $x$   
 123 the turbine speed relative deviation, and  $y$  the wicket gate servomotor stroke relative deviation. In  
 124 particular, in Eq. (3),  $H_r = 400m$  represents the reservoir water level,  $Q_r = 36.13m^3/s$  is the water  
 125 flow rate,  $n_r = 500rpm$  is the rated rotational speed. The hydraulic turbine power is  $P_r = 127.6MW$   
 126 with efficiency rated value  $\eta_r = 0.90$ .

In the following, the non-dimensional performance curves of the hydraulic turbine considered in  
 this work are briefly summarised, as they represent an important nonlinear part of the hydroelectric

plant. In particular, the non-dimensional water flow rate  $Q/Q_r$  is expressed as a function of the non-dimensional rotational speed  $n/n_r$ , and represented by the second order polynomial of Eq. (4):

$$\frac{Q}{Q_r} = G \left[ a_1 \left( \frac{n}{n_r} \right)^2 + b_1 \left( \frac{n}{n_r} \right) + c_1 \right] = f_1(n, G) \quad (4)$$

127 Moreover, the relation of Eq. (4) includes the wicket gate opening, described by the non-dimensional  
 128 parameter  $G$ , varying from 0 to 100%. Fig. 4 represents the curve derived for  $G = 100\%$ , *i.e.* fully open  
 129 wicket gate. Moreover, the curve at  $\eta = 0\%$  is also depicted, thus defining the operating conditions  
 130 of the Francis hydraulic turbine.

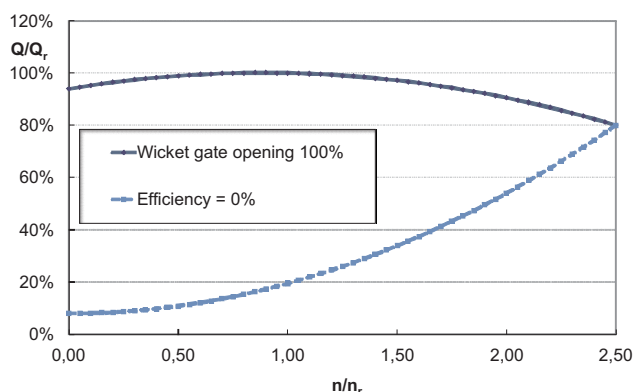


**Figure 4.** Representation of the non-dimensional water flow rate  $Q/Q_r$  with respect to the non-dimensional rotational speed  $n/n_r$ .

131 The variables and parameters of the hydroelectric model were selected according to the work  
 132 [19] in order to represent a realistic hydroelectric plant simulator. Moreover, as for the wind turbine  
 133 benchmark, the signals that can be acquired from the actuator and sensors of the hydroelectric plant  
 134 are modelled as the sum of the actual variables and stochastic noises, as proposed in [7]. For this  
 135 benchmark, a standard PID regulator was proposed to compensate the hydraulic turbine speed  
 136 [19]. Due to its nonlinear characteristics, this solution may lead to unsatisfactory responses, with  
 137 high overshoot and long settling time, as highlighted in [19], since a gain scheduling of the PID  
 138 parameters would have been required. Thus, advanced control strategies that were already proposed  
 139 for the wind turbine benchmark and recalled in Section 3 will be briefly summarised and applied  
 140 to the hydroelectric simulator, as shown in Section 4. Extended simulations, comparisons, and the  
 141 sensitivity analysis of the proposed solutions represent one of the key points of this paper.

142 Finally, it is worth noting that some relations of the hydroelectric system have been linearised,  
 143 see *e.g.* the relations of Eq. (3). However, these simplified models has been considered for comparison  
 144 purpose, as the nonlinear parts of the processes under investigation are closer, as highlighted by Eqs.  
 145 (1) and (4).

### 146 3. Control Techniques for Energy Conversion Systems

147 This section recalls those data-driven and self-tuning control methodologies that will be  
 148 designed and compared when applied to the considered energy conversion benchmark and simulator.  
 149 In general, the control techniques proposed for the systems under investigation should lead to the  
 150 computation of the control law generating the input  $u(t)$  that allows to track the given reference  
 151 or set-point  $r(t)$  for the controlled output  $y(t)$ . For example, the wind turbine system requires the  
 152 computation of the optimal rotational speed ( $\omega_r$  or  $\omega_g$  for the working regions 2 and 3, respectively).  
 153 Moreover, the reference torque  $\tau_r$  and the blade pitch control  $\beta$  are exploited to obtain the needed  
 154 rotational velocity  $\omega_g$ . On the other hand, the hydroelectric system requires an optimal velocity

reference  $n_r$  that is obtained for this plant, and the control of  $u$  and  $y$  allows to track  $n$  according to the desired value  $n_r$ .

The remainder of this section describes briefly several control schemes consisting of self-tuning, data-driven, and Artificial Intelligence (AI) strategies, such as fuzzy logic and adaptive methods, as well as Model Predictive Control (MPC) approach. First, with reference to the process output, the desired transient or steady-state responses can be considered, as for the case of self-tuning PID regulators summarised in Section 3.0.1. On the other hand, if the frequency behaviour is taken into account, the desired closed-loop poles can be fixed as roots of the closed-loop transfer function. This represent the design approach used by the adaptive strategy considered in Section 3.0.3. Moreover, when robust performances are included, the minimisation of the sensitivity of the closed-loop system with respect to the model-reality mismatch or external disturbances can be considered. This approach is related for example to the fuzzy logic methodology reported in Section 3.0.2. Some other strategies provide solutions to this optimisation problem when it is defined at each time step, as for the case of the Model Predictive Control (MPC) with disturbance decoupling considered in Section 3.0.4. The considered strategy integrates the advantages of the MPC solution with the disturbance compensation feature.

Note that some of the control solutions were already proposed by the authors in particular for the wind turbine and wind park installations [20].

### 3.0.1. Self-Tuning PID Control

Industrial processes commonly exploit closed-loop including standard PID controllers, due to their simple structure and parameter tuning [21]. The control law depends on the tracking error  $e(t)$  defined by the difference between the desired and the measured output signals, *i.e.*  $e(t) = r(t) - x(t)$ . This signal is injected into the controlled process after proportional, integral and derivative computations. Therefore, the continuous-time control signal  $u(t)$  is generated by the PID regulator in the form of Eq. (5):

$$u(t) = K_p e(t) + K_i \int_0^t e(\tau) d\tau + K_d \frac{de(t)}{dt} \quad (5)$$

with  $K_p$ ,  $K_i$ ,  $K_d$  being the PID proportional, integral, and derivative gains, respectively. The most common strategy exploited for the computation of the optimal parameters of the PID governor uses proper Ziegler-Nichols formulas [21]. However, with the development of relatively recent automatic software routines, the PID optimal parameters can be easily determined by means of direct tuning algorithms implemented for example in the Simulink environment. These strategies require the definition of the controlled process as Simulink model, such that they balance the input-output performances of the monitored system in terms of response time and stability margins (robustness) [21]. In particular, the PID automatic tuning procedure implemented in the Simulink toolbox performs the computation of the linearised model of the energy conversion systems studied in this paper. The logic scheme of this procedure is sketched in Fig. 5.

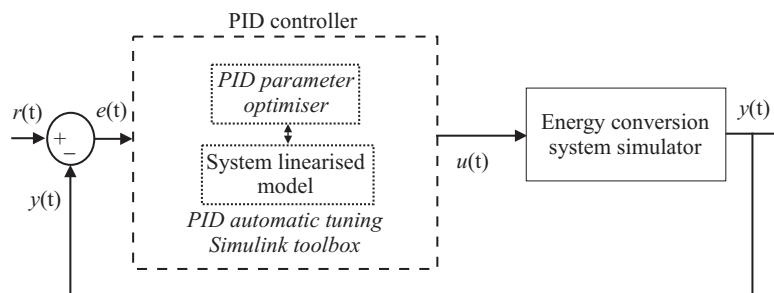


**Figure 5.** Block diagram of the monitored system controlled by the PID regulator with self-tuning feature.



184 Note finally that the PID block in Fig. 5 performs the computation of a linearised model of the  
 185 controlled system, if required. Therefore, the optimiser included in the PID block and implemented in  
 186 the Simulink environment derives of the PID parameters that minimise suitable performance indices,  
 187 as described in [21].

### 188 3.0.2. Data-Driven Fuzzy Control

189 Fuzzy Logic Control (FLC) solutions are often exploited when the dynamics of the monitored  
 190 process are uncertain and can present nonlinear characteristics. The design method proposed in this  
 191 work exploits the direct identification of rule-based Takagi-Sugeno (TS) fuzzy prototypes. Moreover,  
 192 the fuzzy model structure, *i.e.* the number of rules, the antecedents, the consequents and the fuzzy  
 193 membership functions can be estimated by means of the Adaptive Neuro-Fuzzy Inference System  
 194 (ANFIS) toolbox implemented in the Simulink environment [22].

The TS fuzzy prototype relies on a number of rules  $R_i$ , whose consequents are deterministic functions  $f_i(\cdot)$  in the form of Eq. (6):

$$R_i : \text{IF } x \text{ is } A_i \text{ THEN } u_i = f_i(x) \quad (6)$$

where the index  $i = 1, 2, \dots, K$  describes the number of rules  $K$ ,  $x$  is the input vector containing the antecedent variables, *i.e.* the model inputs, whilst  $u_i$  represents the consequent output. The fuzzy set  $A_i$  describing the antecedents in the  $i$ -th rule is described by its (multivariable) membership function  $\mu_{A_i}(x) \rightarrow [0, 1]$ . The relation  $f_i(x)$  assumes the form of parametric affine model represented by the  $i$ -th relation of Eq. (7):

$$u_i = a_i^T x + b_i \quad (7)$$

195 with the vector  $a_i$  and the scalar  $b_i$  being the  $i$ -th submodel parameters. The vector  $x$  consists of  
 196 a proper number  $n$  of delayed samples of input and output signals acquired from the monitored  
 197 process. Therefore, the term  $a_i^T x$  is an Auto-Regressive eXogenous (ARX) parametric dynamic model  
 198 of order  $n$ , and  $b_i$  a bias.

The output  $u$  of the TS fuzzy prototype is computed as weighted average of all rule outputs  $u_i$  in the form of Eq. (8):

$$u = \frac{\sum_{i=1}^K \mu_{A_i}(x) y_i(x)}{\sum_{i=1}^K \mu_{A_i}(x)} \quad (8)$$

199 The estimation scheme implemented by the ANFIS tool follows the classic dynamic system  
 200 identification experiment. First, the structure of the TS fuzzy prototype is defined by selecting a  
 201 suitable order  $n$ , the shape representing the membership functions  $\mu_{A_i}$ , and the proper number of  
 202 clusters  $K$ . Therefore, the input-output data sequences acquired from the monitored system are  
 203 exploited by ANFIS for estimating the TS model parameters and its rules  $R_i$  after the selection of a  
 204 suitable error criterion. The optimal values of the controller parameters represented by the variables  
 205  $a_i$  and  $b_i$  of (7) are thus estimated [23].

206 The work proposes also a strategy different from ANFIS that can be exploited for the estimation  
 207 of the parameters of the fuzzy controller. This method relies on the Fuzzy Modelling and  
 208 Identification (FMID) toolbox designed in the Matlab and Simulink environments as described in  
 209 [24]. Again, the computation of the controller model is performed by estimating the rule-based  
 210 fuzzy system in the form of Eq. (8) from the input-output data acquired from the process under  
 211 investigation. In particular, the FMID tool uses the Gustafson-Kessel (GK) clustering method [24] to  
 212 perform a partition of input-output data into a proper number  $K$  of regions where the local affine  
 213 relations of Eq. (7) are valid. Also in this case, the fuzzy controller model of Eq. (8) is computed  
 214 after the selection of the model order  $n$  and the number of clusters  $K$ . The FMID toolbox derives the  
 215 variables  $a_i$  and  $b_i$ , as well as the identification of the shape of the functions  $\mu_{A_i}$  by minimising a given  
 216 metric [24].

217 Note that the overall digital control scheme consisting of the discrete-time fuzzy regulator of Eq.  
 218 (8) and the controlled system includes also Digital-to-Analog (D/A) and Analog-to-Digital (A/D)  
 219 converters, as shown in Figure 6.

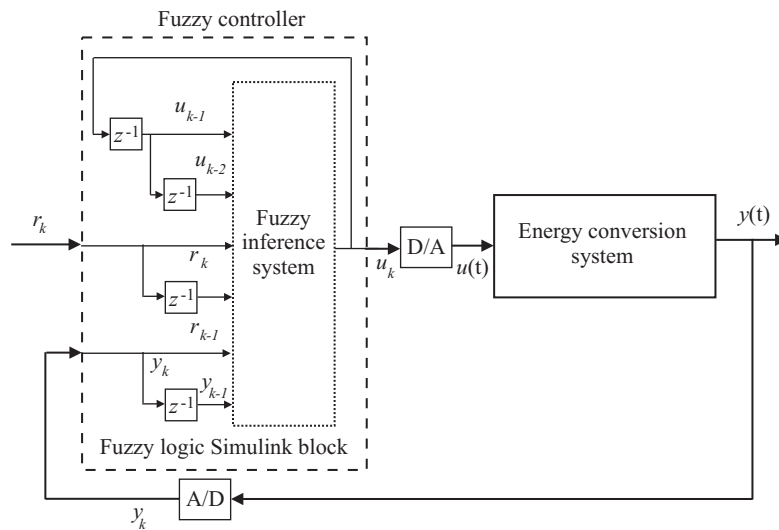


**Figure 6.** Block diagram of the monitored system controlled by the fuzzy regulator.

220 With reference to Figure 6, note finally that the fuzzy controller block implemented in the  
 221 Simulink environment includes a suitable number  $n$  of delayed samples of the signals acquired from  
 222 the monitored process. Moreover, the fuzzy inference system in Figure 6 implements the TS model of  
 223 Eq. (8). The delay  $n$ , the membership functions  $\mu_{A_i}$ , and the number of clusters  $K$  are estimated by  
 224 the FMID and the ANFIS toolboxes, as described in [24].

### 225 3.0.3. Data-Driven Adaptive Control

The adaptive control technique proposed in this work relies on the recursive estimation of a 2-nd order discrete-time transfer function  $G(z)$  with time-varying parameters described by Eq. (9):

$$G(z) = \frac{\beta_1 z^{-1} + \beta_2 z^{-2}}{1 + \alpha_1 z^{-1} + \alpha_2 z^{-2}} \quad (9)$$

226 where  $\alpha_i$  and  $\beta_i$  are identified on-line at each sampling time  $t_k = kT$ , with  $k = 1, 2, \dots, N$ , for  $N$   
 227 samples, and  $T$  being the sampling interval.  $z^{-1}$  indicates the unit delay operator. A viable and  
 228 direct way for deriving the model parameters in Eq. (9) that is proposed in this work is based on the  
 229 Recursive Least-Square Method (RLSM) with directional forgetting factor, which was presented in  
 230 [25].

Once the parameters of the model of Eq. (9) have been derived, this paper proposes to compute the adaptive controller in the form of Eq. (10):

$$u_k = q_0 e_k + q_1 e_{k-1} + q_2 e_{k-2} + (1 - \gamma) u_{k-1} + \gamma u_{k-2} \quad (10)$$

with  $e_k$  and  $u_k$  represent the sampled values of the tracking error  $e(t)$  and the control signal  $u_k$  at the time  $t_k$ , respectively. With reference to the description of Eq. (10), by following a modified Ziegler-Nichols criterion,  $q_0$ ,  $q_1$ ,  $q_2$ , and  $\gamma$  represent the adaptive controller parameters, which are



derived by solving a Diophantine equation. As described in [25], by considering the recursive 2-nd order model of Eq. (9), this technique leads to the relations of Eqs. (11):

$$\begin{cases} q_0 = \frac{1}{\beta_1} (d_1 + 1 - \alpha_1 - \gamma) \\ \gamma = \frac{s_1 \beta_2}{r_1 a_2} \\ q_1 = \frac{\alpha_2}{\beta_2} - \frac{s_1}{r_1} \left( \frac{\beta_1}{\beta_2} - \frac{\alpha_1}{a_2} + 1 \right) \\ q_2 = \frac{s_1}{r_1} \end{cases} \quad (11)$$

where:

$$\begin{cases} r_1 = (b_1 + b_2) (a_1 b_2 b_1 - a_2 b_1^2 - b_2^2) \\ s_1 = a_2 ((b_1 + b_2) (a_1 b_2 - a_2 b_1) + b_2 (b_1 d_2 - b_2 d_1 - b_2)) \end{cases} \quad (12)$$

Note that the design technique proposed in this work and represented by the relations of Eqs. (11) and (12) assumes that the behaviour of the overall closed-loop system can be approximated by a 2nd order transfer function with characteristic polynomial represented by Eq. (13):

$$D(s) = s^2 + 2\delta\omega s + \omega^2 \quad (13)$$

with  $\delta$  and  $\omega$  being the damping factor and natural frequency, respectively.  $s$  is the derivative operator. Furthermore, if  $\delta \leq 1$ , the following relations are used [25]:

$$\begin{cases} d_1 = -2e^{-\delta\omega T} \cos(\omega T \sqrt{1 - \delta^2}) \\ d_2 = e^{-2\delta\omega T} \end{cases} \quad (14)$$

231 The on-line control law of Eq. (10) is used for the regulation of the continuous-time nonlinear system  
232 by including D/A and A/D converters, as highlighted in the scheme of Figure 7.

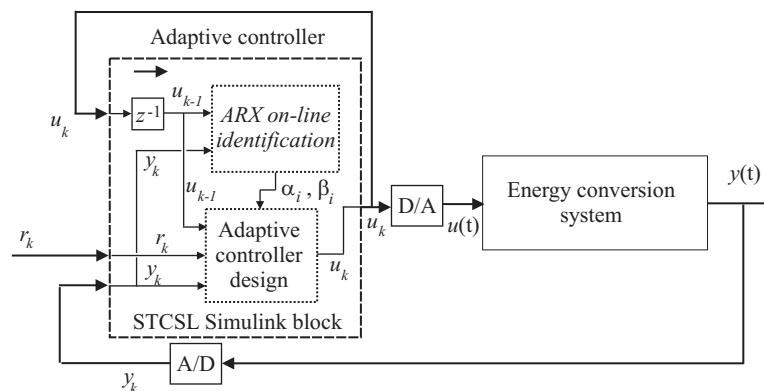
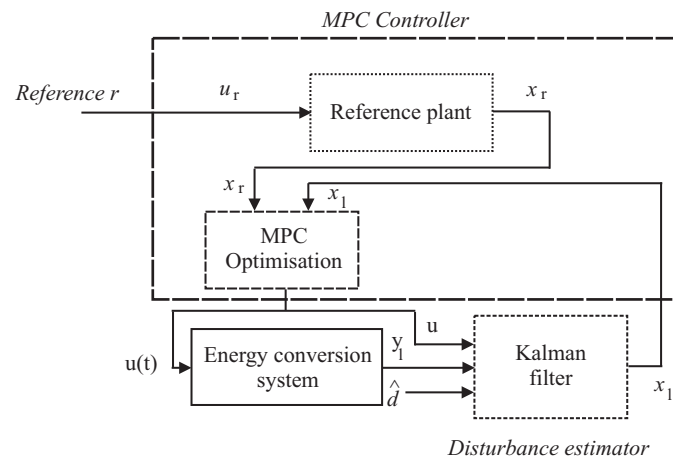


Figure 7. Block diagram of the monitored system controlled by the adaptive regulator.

233 Note finally that the adaptive control sketched in Figure 7 is implemented via the Self-Tuning  
234 Controller Simulink Library (STCSL) block in the Simulink environment. It includes the module  
235 performing the on-line identification of the ARX model of Eq. (9), which is used for the adaptive  
236 controller design in the form of Eq. (10) [25].

### 3.0.4. Model Predictive Control with Disturbance Decoupling

The general structure of the proposed Model Predictive Control (MPC) is illustrated in Figure 8, with the MPC managing objectives and constraints of the control inputs. The MPC works as a standard MPC controller when the nominal plant is considered, and generates the reference inputs. In the presence of disturbance or uncertainty effects, the considered solution provides the reconstruction of the equivalent disturbance signal acting on the plant. This represents the key feature of this structure, which compensates the disturbance effect and 'hide' it to the overall system. In this way, it decouples the disturbance effect from the nominal MPC design.



**Figure 8.** Block diagram of the disturbance compensated MPC scheme.

The overall scheme is thus represented aim by the MPC design with disturbance compensation, such that the compensated system has response very similar to the nominal system and the constraints are not violated. The fault compensation problem within the MPC framework is defined as follows. Given a state–space representation of the considered system affected by disturbance or uncertainty has the following form:

$$\begin{cases} \dot{x}_l = A_l x_l + B_l u + B_d d + w \\ y_l = C_l x_l + v \end{cases} \quad (15)$$

and its nominal reference model:

$$\begin{cases} \dot{x}_r = A_l x_r + B_l u_r \\ y_r = C_l x_r \end{cases} \quad (16)$$

the disturbance compensation problem is solved by finding the control input  $u$  that minimises the cost function:

$$J = \int_t^{t+N_c \Delta t} \left( \|x_l - x_r\|_Q^2 + \|\dot{u}\|_R^2 \right) d\tau \quad (17)$$

given the reference input  $u_r$ .

In Eq. (15) the matrices  $A_l$ ,  $B_l$ ,  $B_d$  and  $C_l$  are of proper dimensions. The vector  $y_l$  represents the output measurements,  $x_l$  is the state of the model with disturbance, whilst  $x_r$  is the reference state, and  $y_r$  the reference output, corresponding to the reference input  $u_r$  of the nominal model. The vectors  $w$  and  $v$  include the model mismatch and the measurement error, respectively.  $d$  represents the equivalent disturbance signal. In Eq. (17)  $t$  is the current time,  $\Delta t$  is the control interval, and  $N_c$  is the length of the control horizon.  $Q$  and  $R$  are suitable weighting matrices. Note that the model of Eq. (15) can be derived by nonlinear model linearisation or identification procedures, as suggested in Sections 3.0.1 and 3.0.3, respectively.

This work proposes to solve the problem in two steps: the reconstruction of the disturbance  $d$ , i.e.  $\hat{d}$ , provided by the disturbance estimation module, and the MPC tool. Due to the model–reality mismatch and the measurement error in (15), the Kalman filter (18) is used to provide the estimation of the state vector  $x_l$ , the output  $y_l$  of the system affected by the estimated disturbance  $\hat{d}$ :

$$\begin{cases} \dot{x}_l &= A_l x_l + B_l u - B_l \hat{d} + K_f (y_l - C_l x_l) \\ y_l &= C_l x_l \end{cases} \quad (18)$$

where  $K_f$  is the Kalman filter gain. In this way, based on the estimations  $\hat{d}$  and  $x_l$ , an MPC is designed, which contains the reference model of Eq. (16) and the filtered system of Eq. (18), with  $\hat{d}$  provided by the Kalman filter. Moreover, the MPC has the objective function:

$$\int_t^{t+N_c \Delta t} \left[ (x_l - x_r)^T Q (x_l - x_r) + \dot{u}^T R \dot{u} \right] d\tau \quad (19)$$

254 in which  $x_l$  and  $x_r$  are the states of the filtered and the reference models, respectively. The integrated  
 255 MPC with the Kalman filter solves this general disturbance compensation problem, as long as the  
 256 estimations of both the state and the disturbance are correct. An illustration of the structure of the  
 257 fault compensated MPC is shown in Figure 8.

258 The global estimation and control scheme is a nonlinear MPC problem with the nominal model  
 259 for the considered energy conversion systems of Eq. (15), the disturbance  $d$  with its estimator,  
 260 and the Kalman filter of Eq. (18) as prediction model. The local observability of the model of Eq.  
 261 (15) is essential for state estimation, which is easily verified. The implementation of the proposed  
 262 disturbance compensation strategy has been integrated into the MPC Toolbox of the Simulink  
 263 environment.

#### 264 4. Simulation Results

The results obtained with the application of the developed control techniques are evaluated via the percent Normalised Sum of Squared Error (NSSE%) performance function in the form of Eq. (20):

$$NSSE\% = 100 \sqrt{\frac{\sum_{k=1}^N (r_k - o_k)^2}{\sum_{k=1}^N r_k^2}} \quad (20)$$

265 with  $r_k$  being the sampled reference or set–point  $r(t)$ , whilst  $o_k$  is the sampled continuous–time signal  
 266 representing the generic controlled output  $y(t)$  of the process. In particular, this signal is represented  
 267 by the wind turbine generator angular velocity  $\omega_g(t)$  in Eq. (2), and the hydraulic turbine rotational  
 268 speed  $n$  in Eq. (3) for the hydroelectric plant.

269 Note that the wind turbine benchmark and the hydroelectric plant simulator of Section 2 allow  
 270 the generation of several input–output data sequences due to different wind speed  $v(t)$  effects and  
 271 hydraulic transient under variable loads, respectively. Moreover, in order to obtain comparable  
 272 working situations, the wind turbine benchmark has been operating from partial to full load  
 273 conditions (from region 2 to region 3). It is thus considered the similar maneuver of the hydroelectric  
 274 system operating from the start–up to full load working condition. After these considerations, Section  
 275 4.1 summarises the results obtained from the wind turbine benchmark first. Then, the same control  
 276 techniques will be verified when applied to the hydroelectric simulator.

##### 277 4.1. Control Technique Performances and Comparisons

278 Figure 9 reports the results achieved with the control methodologies and the tools summarised  
 279 in Section 3. In particular, Figure 9 depicts the wind turbine generator angular velocity  $\omega_g$  when the  
 280 wind speed  $v(t)$  changes from  $3m/s$  to  $18m/s$  for a simulation time of 4400s [6].

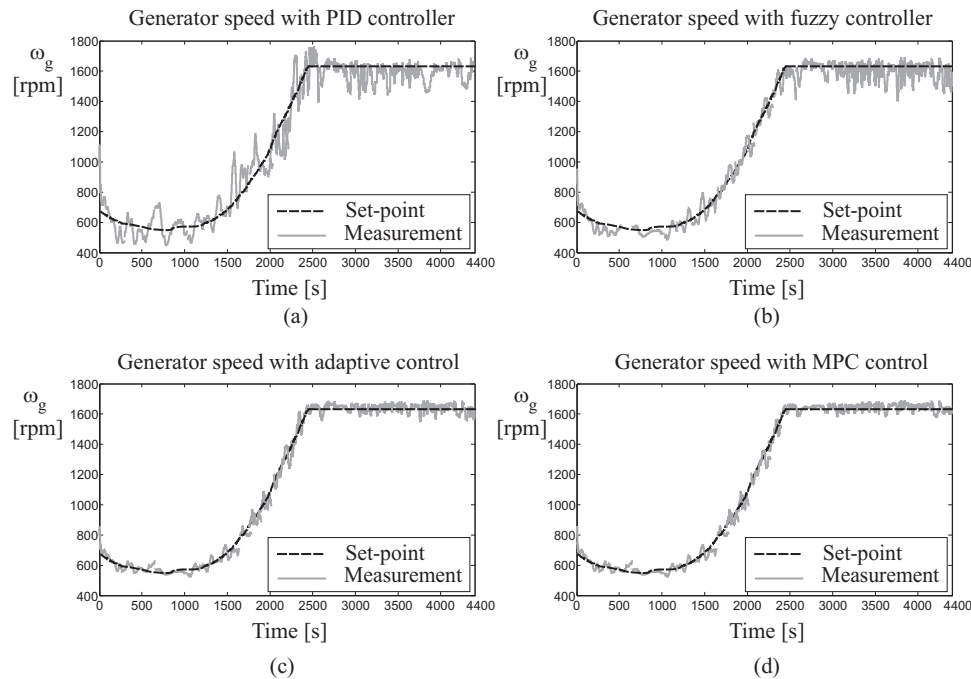


**Figure 9.** Wind turbine controlled output compensated by (a) the self-tuning PID regulator, (b) the fuzzy controller, (c) the adaptive regulator, and (d) the MPC approach with disturbance decoupling.

281 In detail, with reference to the picture in Figure 9 (a), the parameters of the PID regulator of Eq.  
 282 (5) have been determined using the self-tuning tool available in the Simulink environment. They  
 283 were settled to  $K_p = 4.0234$ ,  $K_i = 1.0236$ ,  $K_d = 0.0127$ . The achieved performances are better than the  
 284 ones obtained with the baseline control laws proposed in [6].

285 Moreover, Figure 9 (b) shows the simulations achieved with the data-driven fuzzy identification  
 286 approach recalled in Section 3.0.2. In particular, a sampling interval  $T = 0.01s$  has been exploited,  
 287 and the TS fuzzy controller of Eq. (8) has been obtained for a number  $K = 3$  of Gaussian membership  
 288 functions, and a number  $n = 2$  of delayed inputs and output. The antecedent vector in Eq. (7) is  
 289 thus  $x = [e_k, e_{k-1}, e_{k-2}, u_{k-1}, u_{k-2}]$ . Both the data-driven FMID and ANFIS tools available in the  
 290 Matlab and Simulink environments provide also the optimal identification of the shapes of the fuzzy  
 291 membership functions  $\mu_{A_i}$  of the fuzzy sets  $A_i$  in Eq. (6).

292 On the other hand, the picture in Figure 9 (c) shows the capabilities of the adaptive controller of  
 293 Eq. (10). The time-varying parameters of this data-driven control technique summarised in Section  
 294 3.0.3 have been computed on-line via the relations of Eqs. (11) with the damping factor and the  
 295 natural frequency variables  $\delta = \omega = 1$  in Eq. (13).

296 Finally, the picture of Figure 9 (d) highlights the results achieved with the MPC technique with  
 297 disturbance decoupling recalled in Section 3.0.4. The state-space model of the wind turbine nonlinear  
 298 system of Eq. (2) exploited for the design of the MPC and the Kalman filter for the estimation of the  
 299 disturbance has order  $n = 5$ , with a prediction horizon  $N_p = 10$  and a control horizon  $N_c = 2$ . The  
 300 weighting factors have been settled to  $w_{y_k} = 0.1$  and  $w_{u_k} = 1$ , in order to reduce possible abrupt  
 301 changes of the control input. Note that, in this case, the MPC technique has led to the best results,  
 302 since it exploits a disturbance decoupling strategy, whilst its parameters have been iteratively adapted  
 303 in the Simulink environment in order to optimise the MPC cost function of Eq. (17), as addressed in  
 304 Section 3.0.4.

305 The second test case regards the hydroelectric plant simulator, where the hydraulic system  
 306 with its turbine speed governor generates hydraulic transients due to the load changes. In order  
 307 to consider operating situations similar to the wind turbine benchmark, the capabilities of the

308 considered control techniques applied to the hydroelectric simulator have been evaluated during  
 309 the start-up to full load maneuver. Moreover, an increasing load torque has been imposed during the  
 310 start-up to full load phase, which is assumed to last 300s because of the large size of the considered  
 311 Francis turbine, and for a simulation of 900s.

312 Under these assumptions, Figure 10 summarises the results achieved with the application of  
 313 the control strategies recalled in Section 3. In particular, for all cases, Figure 10 highlights that the  
 314 hydraulic turbine angular velocity  $n$  increases with the load torque  $m_{g0}$  during the start-up to full  
 315 working condition maneuver.

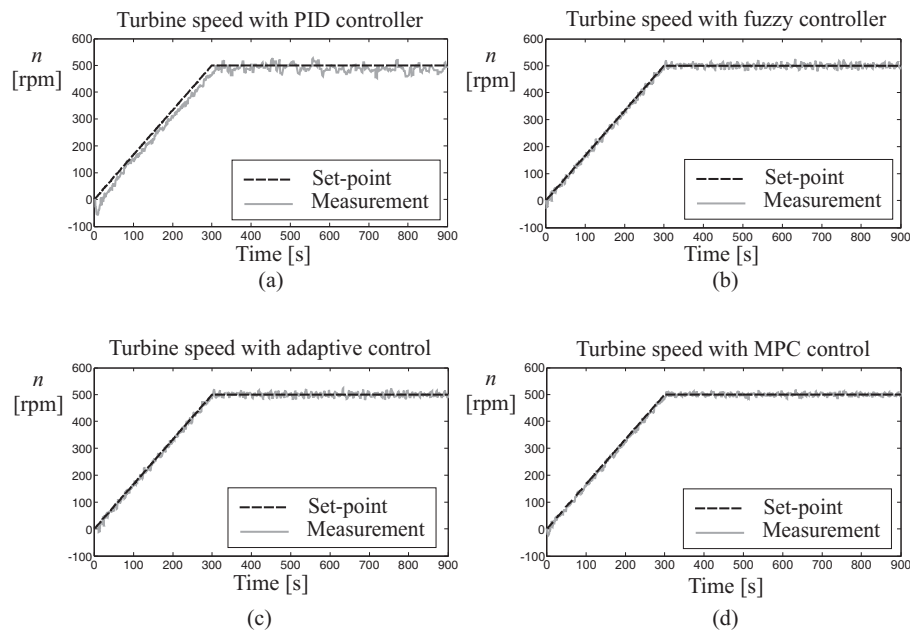


**Figure 10.** Hydroelectric system with (a) the self-tuning PID regulator, (b) the fuzzy controller, (c) the adaptive regulator, and (d) the MPC approach with disturbance decoupling.

316 In more detail, Figure 10 (a) shows the performance of the PID regulator when its parameters are  
 317 determined via the self-tuning procedure recalled in Section 3.0.1. Furthermore, Figure 10 (a) shows  
 318 that the PID governor with self-tuning capabilities is able to keep the hydraulic turbine rotational  
 319 speed error  $n - n_r$  null ( $r(t) = n_r$ , *i.e.* the rotational speed constant) in steady-state conditions.

320 Figure 10 (b) reports the results concerning the TS fuzzy controller described by Eq. (8) in Section  
 321 3.0.2. This fuzzy controller was implemented for a sampling interval  $T = 0.1s$ , with a number  $K = 2$  of  
 322 Gaussian membership functions, and a number  $n = 3$  of delayed inputs and output. The antecedent  
 323 vector exploited by the relation of Eq. (7) is thus  $x = [e_k, e_{k-1}, e_{k-2}, e_{k-3}, u_{k-1}, u_{k-2}, u_{k-3}]$ .  
 324 Moreover, as recalled in Section 3.0.2, the data-driven FMID and ANFIS tools implemented in the  
 325 Simulink toolboxes are able to provide the estimates of the shapes of the membership functions  $\mu_{A_i}$   
 326 used in Eq. (8).

327 On the other hand, Figure 10 (c) reports the simulations obtained via the data-driven adaptive  
 328 controller of Eq. (10), whose time-varying parameters are computed by means of the relations of  
 329 Eqs. (11). The damping factor and the natural frequency parameters used in Eq. (13) were selected  
 330 as  $\delta = \omega = 1$ . The STCSL tool described in Section 3.0.3 implements this data-driven adaptive  
 331 technique using the on-line identification of the input-output model of Eq. (9) [25].

332 Finally, regarding the MPC technique with disturbance decoupling proposed in Section 3.0.4,  
 333 Fig. 10 (d) reports the simulations obtained using a prediction horizon  $N_p = 10$  and a control horizon  
 334  $N_c = 2$ . Also in this case, the weighting parameters have been fixed to  $w_{y_k} = 0.1$  and  $w_{u_k} = 1$ , in  
 335 order to limit fast variations of the control input, as it will be remarked in the following. Furthermore,

the MPC design was performed using a linear state–space model for the nonlinear hydroelectric plant simulator of order  $n = 6$ .

In order to provide a quantitative comparison of the tracking capabilities obtained by the considered control techniques for the wind turbine benchmark, the first row in Table 1 summarises the achieved results in terms of *NSSE%* index.

**Table 1.** Performance of the considered control solutions.

Simulated system	Working Condition	Standard PID	Self-tuning PID	Fuzzy PID	Adaptive PID	MPC Scheme
Wind turbine	From partial to full load	11.5%	7.3%	5.7%	4.1%	2.8%
Hydro plant	From start-up to full load	6.2%	4.9%	3.1%	1.8%	0.9%

In particular, the *NSSE%* values in the first row of Table 1 highlight better capabilities of the proposed fuzzy controllers with respect to the PID regulators with self-tuning feature. This is motivated by the better flexibility and generalisation capabilities of the fuzzy tool, and in particular the FMID toolbox proposed in [24]. A better behaviour is obtained by means of the adaptive solution, due to its inherent adaptation mechanism, which allows to track the reference signal in the different working conditions of the wind turbine process. However, the MPC technique with disturbance decoupling has led to the best results, as reported in the first row of Table 1, since is able to optimise the overall control law over the operating conditions of the system, by taking into account future operating situations of its behaviour. while compensating the disturbance effects.

On the other hand, the results achieved by the validation of the considered control techniques to the hydroelectric plant simulator are summarised in the second row of Table 1. In this case, the values of the *NSSE%* function are evaluated for the considered conditions of varying load torque  $m_{g0}$  corresponding to the plant start-up to full load maneuver. According to these simulation results, good properties of the proposed self-tuning PID regulator are obtained, and they are better than the baseline PID governor with fixed gains developed in [19]. In fact, the self-tuning design feature of the Simulink environment is able to limit the effect of high-gains for the proportional and the integral contributions of the standard PID control law. On the other hand, the data-driven fuzzy regulator has led to even better results, which are outperformed by the adaptive solution. However, also for the case of the hydroelectric plant simulator, the best performances are obtained by means of the MPC strategy with disturbance decoupling. Note that, with reference to Table 1, the comparison should be performed by considering the *NSSE%* values for a given plant. In fact, even if the *NSSE%* index assumes quite similar values, it refers to control techniques implemented and applied to different processes.

Finally, in order to highlight some further features of the considered, the controlled inputs applied to the wind turbine system are depicted and compared in Figures 11 (a) and (c), whilst the one feeding the hydroelectric plant in Figure 11 (b) and (d). For the sake of brevity, only the data-driven fuzzy controller and the MPC with disturbance decoupling have been summarised here.

By considering these control inputs, with reference to the data-driven methodologies, and in particular to the design of the fuzzy controllers, off-line optimisation strategies allow to reach quite good results. However, control inputs are subjected to faster variations. Other control techniques can take advantage of more complicated and not direct design methodologies, as highlighted by the MPC scheme. In this case, due to the input constraint, its changes are reduced. This feature is attractive for wind turbine systems, where variations of the control inputs must be limited. This represents another important benefit of MPC with disturbance decoupling, which integrates the advantages of the classic MPC scheme with disturbance compensation effects. Therefore, with reference to these two



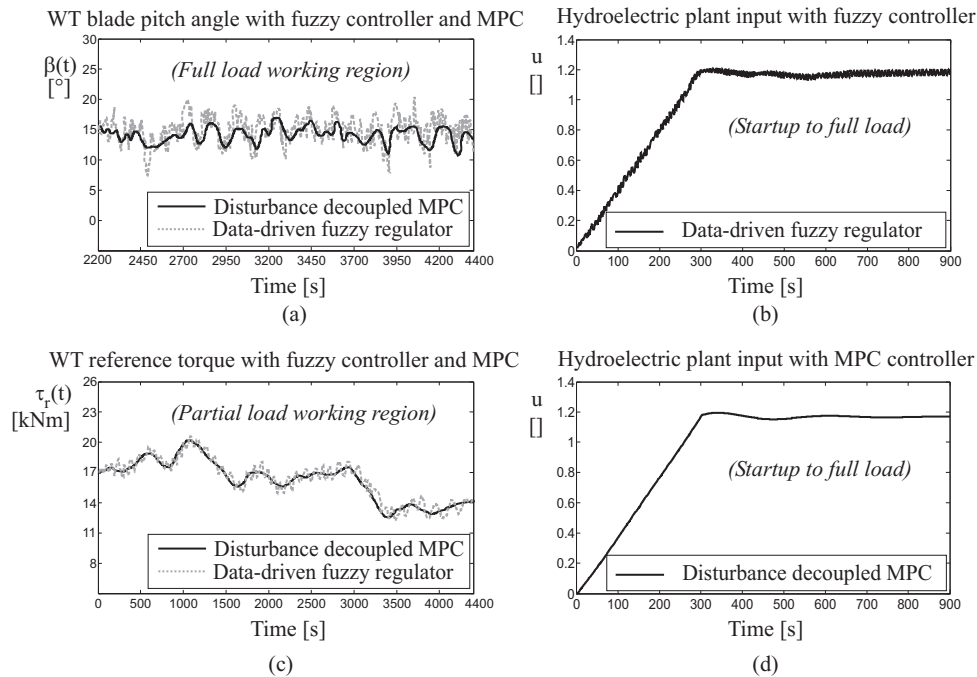


**Figure 11.** Wind turbine (a), (c) and hydroelectric plant (b), (d) compensated by the fuzzy controller and the MPC approach with disturbance decoupling.

control methods, they can appear rather straightforward, even if further optimisation and estimation strategies have to be applied.

#### 4.2. Sensitivity Analysis

This section analyses the reliability and robustness properties of the developed controllers when parameter variations and measurement errors are considered. This further investigation relies on the Monte–Carlo tool, since the control behaviour and the tracking capabilities depend on both the model–reality mismatch effects and the input–output uncertainty levels. Therefore, this analysis has been implemented by describing the parameters of both the wind turbine system and hydroelectric plant models as Gaussian stochastic processes with average values corresponding to the nominal ones summarised in Table 2 for the wind turbine benchmark.

**Table 2.** Wind turbine benchmark parameters for the sensitivity analysis.

Variable	$R$	$\chi$	$\omega_n$	$B_{dt}$	$B_r$
Nominal value	57.5 m	0.6	106,09 rpm	775.49 N m s rad <sup>-1</sup>	7.11 N m s rad <sup>-1</sup>
Variable	$B_g$	$K_{dt}$	$\eta_{dt}$	$J_g$	$J_r$
Nominal value	45.6 N m s rad <sup>-1</sup>	$2.7 \cdot 10^9$ N m rad <sup>-1</sup>	0.97	390 kg m <sup>2</sup>	$55 \cdot 10^6$ kg m <sup>2</sup>

Moreover, Table 2 shows that these model parameters have standard deviations of  $\pm 30\%$  of the corresponding nominal values [6].

On the other hand, Table 3 reports the hydroelectric simulator model variables with their nominal values varied by  $\pm 30\%$  in order to develop the same Monte–Carlo analysis [7].

Therefore, the average values of  $NSSE\%$  index have been thus evaluated by means of 1000 Monte–Carlo simulations. They have been reported in Tables 4 and 5 for the wind turbine benchmark and the hydroelectric plant simulator, respectively.

**Table 3.** Hydroelectric simulator parameters for the sensitivity analysis.

<b>Variable</b>	<i>a</i>	<i>b</i>	<i>c</i>	$H_{f_1}$	$H_{f_3}$	$H_{f_5}$	$T_a$
<b>Nominal value</b>	-0.08	0.14	0.94	0.0481 m	0.0481 m	0.0047 m	5.9 s
<b>Variable</b>	$T_c$	$T_{s_2}$	$T_{s_4}$	$T_{w_1}$	$T_{w_3}$	$T_{w_5}$	
<b>Nominal value</b>	20 s	476.05 s	5000 s	3.22 s	0.83 s	0.1 s	

**Table 4.** Sensitivity analysis applied to the wind turbine benchmark.

Standard PID	Self-tuning PID	Fuzzy PID	Adaptive PID	MPC Scheme
13.8%	9.2%	7.6%	5.3%	3.9%

**Table 5.** Sensitivity analysis applied to the hydroelectric plant simulator.

Standard PID	Self-tuning PID	Fuzzy PID	Adaptive PID	MPC Scheme
9.1%	7.4%	5.6%	3.5%	2.2%

393 It is worth noting that the results summarised in Tables 4 and 5 serve to verify and validate  
 394 the overall behaviour of the developed control techniques, when applied to the considered wind  
 395 turbine benchmark and hydroelectric plant simulator, respectively. In more detail, the values of the  
 396 *NSSE%* index highlights that when the mathematical description of the controlled dynamic processes  
 397 can be included in the control design phase, the MPC technique with disturbance decoupling still  
 398 yields to the best performances, even if an optimisation procedure is required. However, when  
 399 modelling errors are present, the off-line learning exploited by the data-driven fuzzy regulators  
 400 allows to achieve results better than model-based schemes. For example, this consideration is  
 401 valid for the PID controllers derived via the self-tuning procedure. On the other hand, fuzzy  
 402 controllers have led to interesting tracking capabilities. With reference to the data-driven adaptive  
 403 scheme, it takes advantage of its recursive features, since it is able to track possible variations of  
 404 the controlled systems, due to operation or model changes. However, it requires quite complicated  
 405 and not straightforward design procedures relying on data-driven recursive algorithms. Therefore,  
 406 fuzzy-based schemes use the learning accumulated from data-driven off-line simulations, but the  
 407 training stage can be computationally heavy. Finally, concerning the standard PID control strategy, it  
 408 is rather simple and straightforward. Obviously, the achievable performances are quite limited when  
 409 applied to nonlinear dynamic processes. Note that they were proposed as baseline control solutions  
 410 for the considered processes. It can be thus concluded that the proposed data-driven self-tuning  
 411 approaches seem to represent powerful techniques able to cope with uncertainty, disturbance and  
 412 variable working conditions. Note finally that the plant simulators, the control solutions, and the data  
 413 exploited for the analysis addressed in this paper are directly and freely available from the authors.

## 414 5. Conclusions

415 The work considered two renewable energy conversion systems, such as a wind turbine  
 416 benchmark and a hydroelectric plant simulator, together with the development of proper data-driven  
 417 control techniques. In particular, the three-bladed horizontal axis wind turbine benchmark  
 418 reported in this work consisted of simple models of the gear-box, the drive-train, and the electric  
 419 generator/converter. On the other hand, the hydroelectric plant simulator included a high water  
 420 head, a long penstock with upstream and downstream surge tanks, and a Francis hydraulic turbine.

Standard PID governors were earlier developed for these processes, which were rather simple and straightforward, but with limited achievable performances. Therefore, the paper proposed different control strategies mainly relying on data-driven approaches. Their performances were analysed first. Then, the reliability and robustness of these solutions were also verified and validated with respect to parameter variations of the plant models and measurement errors, via the Monte-Carlo tool. The achieved results highlighted that data-driven approaches, such as the fuzzy regulators were able to provide good tracking performances. However, they were easily outperformed by adaptive and model predictive control schemes, representing data-driven solutions that require optimisation stages, adaptation procedures and disturbance compensation methods. Future investigations will consider the verification and the validation of the considered control techniques when applied to higher fidelity simulators of energy conversion systems.

**Sample Availability:** The software codes for the proposed control strategies, the simulated benchmarks and the generated data are available from the authors on demand in the Matlab and Simulink environments.

**Acknowledgments:** The research works have been supported by the FAR2018 local fund from the University of Ferrara. On the other hand, the costs to publish in open access have been covered by the FIR2018 local fund from the University of Ferrara.

**Author Contributions:** Silvio Simani conceived and designed the simulations. Silvio Simani analysed the methodologies, the achieved results, and together with Stefano Alvisi and Mauro Venturini, wrote the paper.

**Conflicts of Interest:** The authors declare no conflicts of interest.

## Bibliography

1. Tetu, A.; Ferri, F.; Kramer, M.B.; Todalshaug, J.H. Physical and Mathematical Modeling of a Wave Energy Converter Equipped with a Negative Spring Mechanism for Phase Control. *Energies* **2018**, *11*, 2362. DOI: 10.3390/en11092362.
2. Hassan, M.; Balbaa, A.; Issa, H.H.; El-Amary, N.H. Asymptotic Output Tracked Artificial Immunity Controller for Eco-Maximum Power Point Tracking of Wind Turbine Driven by Doubly Fed Induction Generator. *Energies* **2018**, *11*, 2632. DOI: 10.3390/en11102632.
3. Fernandez-Guillamon, A.; Villena-Lapaz, J.; Viguera-Rodriguez, A.; Garcia-Sanchez, T.; Molina-Garcia, A. An Adaptive Frequency Strategy for Variable Speed Wind Turbines: Application to High Wind Integration into Power Systems. *Energies* **2018**, *11*, 1436. DOI: 10.3390/en11061436.
4. Blanco-M., A.; Gibert, K.; Marti-Puig, P.; Cusido, J.; Sole-Casals, J. Identifying Health Status of Wind Turbines by using Self Organizing Maps and Interpretation-Oriented Post-Processing Tools. *Energies* **2018**, *11*, 723. DOI: 10.3390/en11040723.
5. World Energy Council., Ed. *Cost of Energy Technologies*; World Energy Perspective, World Energy Council: London, UK, 2018. ISBN: 9780946121304. Available at: [www.worldenergy.org](http://www.worldenergy.org).
6. Odgaard, P.F.; Stoustrup, J.; Kinnaert, M. Fault-Tolerant Control of Wind Turbines: A Benchmark Model. *IEEE Transactions on Control Systems Technology* **2013**, *21*, 1168–1182. ISSN: 1063–6536. DOI: 10.1109/TCST.2013.2259235.
7. Simani, S.; Alvisi, S.; Venturini, M. Fault Tolerant Control of a Simulated Hydroelectric System. *Control Engineering Practice* **2016**, *51*, 13–25. DOI: <http://dx.doi.org/10.1016/j.conengprac.2016.03.010>.
8. Honrubia-Escribano, A.; Gomez-Lazaro, E.; Fortmann, J.; Sorensen, P.; Martin-Martinez, S. Generic dynamic wind turbine models for power system stability analysis: A comprehensive review. *Renewable and Sustainable Energy Reviews* **2018**, *81*, 1939–1952. DOI: 10.1016/j.rser.2017.06.005.
9. Singh, V.K.; Singal, S.K. Operation of hydro power plants—a review. *Renewable and Sustainable Energy Reviews* **2017**, *69*, 610–619. DOI: 10.1016/j.rser.2016.11.169.
10. Bianchi, F.D.; Battista, H.D.; Mantz, R.J. *Wind Turbine Control Systems: Principles, Modelling and Gain Scheduling Design*, 1st ed.; Advances in Industrial Control, Springer, 2007. ISBN: 1–84628–492–9.
11. Kishor, N.; Saini, R.; Singh, S. A review on hydropower plant models and control. *Renewable and Sustainable Energy Reviews* **2007**, *11*, 776–796.
12. Hanmandlu, M.; Goyal, H. Proposing a new advanced control technique for micro hydro power plants. *International Journal of Electrical Power & Energy Systems* **2008**, *30*, 272–282.

- 471 13. Kishor, N.; Singh, S.; Raghuvanshi, A. Dynamic simulations of hydro turbine and its state estimation  
472 based LQ control. *Energy Conversion and Management* **2006**, *47*, 3119–3137.
- 473 14. Mahmoud, M.; Dutton, K.; Denman, M. Design and simulation of a nonlinear fuzzy controller for a  
474 hydropower plant. *Electric Power Systems Research* **2005**, *73*, 87–99.
- 475 15. Sarasua, J.I.; Martinez-Lucas, G.; Platero, C.A.; Sanchez-Fernandez, J.A. Dual Frequency Regulation  
476 in Pumping Mode in a Wind–Hydro Isolated System. *Energies* **2018**, *11*, 1996–1073. DOI:  
477 10.3390/en11112865.
- 478 16. Martinez-Lucas, G.; Sarasua, J.I.; Sanchez-Fernandez, J.A. Eigen analysis of wind–hydro joint frequency  
479 regulation in an isolated power system. *International Journal of Electrical Power & Energy Systems* **2018**,  
480 *103*, 511–524. DOI: 10.1016/j.ijepes.2018.06.028.
- 481 17. Popescu, M.; Arsenie, D.; Vlase, P. *Applied Hydraulic Transients: For Hydropower Plants and Pumping*  
482 *Stations*; CRC Press: Lisse, The Netherlands, 2003.
- 483 18. de Mello, F.P.; Koessler, R.J.; Agee, J.; Anderson, P.M.; Doudna, J.H.; Fish, J.H.; Hamm, P.A.L.; Kundur, P.;  
484 Lee, D.C.; Rogers, J.; Taylor, C. Hydraulic turbine and turbine control models for system dynamic studies.  
485 *IEEE Transactions on Power Systems* **1992**, *7*, 167–179. DOI: 10.1109/59.141700.
- 486 19. Fang, H.; Chen, L.; Dlakavu, N.; Shen, Z. Basic Modeling and Simulation Tool for Analysis of Hydraulic  
487 Transients in Hydroelectric Power Plants. *IEEE Trans. Energy Convers.* **2008**, *23*, 424–434.
- 488 20. Simani, S.; Farsoni, S. *Fault Diagnosis and Sustainable Control of Wind Turbines: Robust data-driven and*  
489 *model-based strategies*, 1st ed.; Mechanical Engineering, Butterworth–Heinemann – Elsevier: Oxford (UK),  
490 2018. ISBN: 9780128129845.
- 491 21. Åström, K.J.; Hägglund, T. *Advanced PID Control*; ISA - The Instrumentation, Systems, and Automation  
492 Society: Research Triangle Park, NC 27709, 2006. ISBN: 978–1–55617–942–6.
- 493 22. Jang, J.S.R. ANFIS: Adaptive–Network–based Fuzzy Inference System. *IEEE Transactions on Systems,*  
494 *Man., & Cybernetics* **1993**, *23*, 665–684.
- 495 23. Jang, J.S.R.; Sun, C.T. *Neuro–Fuzzy and Soft Computing: A Computational Approach to Learning and Machine*  
496 *Intelligence*, 1st ed.; Prentice Hall, 1997. ISBN: 9780132610667.
- 497 24. Babuška, R. *Fuzzy Modeling for Control*; Kluwer Academic Publishers: Boston, USA, 1998.
- 498 25. Bobál, V.; Böhm, J.; Fessl, J.; Macháček, J. *Digital Self-Tuning Controllers: Algorithms, Implementation and*  
499 *Applications*, 1st ed.; Advanced Textbooks in Control and Signal Processing, Springer, 2005.